Numerical Simulation and Air Conditioning System Improvement for the Experimental Hall at TLS

J.C. Chang[a], M.T. Ke[b], Z.D. Tsai[a], and J. R. Chen[a]
[a] National Synchrotron Radiation Research Center (NSRRC)
101 Hsin-Ann Rd., Science Park, Hsinchu 30076, Taiwan
[b] Graduate Institute of Air-Conditioning and Refrigeration Engineering, National Taipei University of Technology, Taipei 106, Taiwan

Abstract

This paper presents the air temperature analysis and control improvement for the experimental hall at the Taiwan Light Source (TLS). The inner and outer diameters and height of the donut-shaped experimental hall are 29m, 80m and 11.7m, respectively. Total seventy-two temperature sensors are installed in this zone, where sixty sensors are installed along the beamlines to on-line record the air temperature history. Because more and more experimental apparatuses were installed in the experimental hall, the cooling capacity of the air-conditioning (AC) system became insufficient for both experimental thermal requirements and human comfort. The temporal temperature variation may be more than 2 degree C in one day. The spatial temperature difference is also about 2 degree C. To cope with those problems, a computational fluid dynamics (CFD) code is applied to simulate the 3-dimensional temperature distribution in the experimental hall. The AC cooling capacity had also been increased accordingly to improve the temperature control in the experimental hall last year.

1. Introduction

According to the study of utility effects on the beam stability, thermal effect is the most critical mechanical factor affecting the beam stability[1][2]. The TLS has made a serious of improvements on the air temperature control for the storage ring. Computational Fluid Dynamics (CFD) technique was applied on the simulation for the air-cooling magnet lattice girder [3]. Mini environment control technique for the elliptical polarization undulator was implemented [4]. The air temperature control for the storage ring tunnel was improved in 2003 [5] and the temperature distribution and the flow field was numerically simulated in 2005 [6]. The air temperature variation in the storage ring tunnel is globally controlled within $\pm$ 0.1^{o}C currently.

However, the cooling capacity of the storage experimental hall was decrease due to improvement in the AC system of the storage ring tunnel. Formerly, there were total four identical air handling units (AHU) serving for two main areas of the storage ring building, i.e., the storage ring tunnel and the experimental hall. The AC systems of these two areas were decoupled and each area was then supplied by two identical AHUs in the AC system modification in 2003[5]. Because the cooling space of the experimental hall is much larger than that of the storage tunnel, the cooling capacity of the storage ring tunnel was increased but that of the experimental hall was decrease. Furthermore, more and more equipment and experimental apparatus, including one cryogenics flat and some protein beamlines, were added in the experimental hall to perform some research of state of the art. At the end of 2005, there are thirty beamlines and seventy end-stations located in the experimental hall. Those new added cooling loads worsen the insufficiency of the cooling capacity for the experimental hall. On the other hand, the experimental stability requirements are more critical then ever. To cope with this AC issue, we conducted some measurements and performed CFD technique to analysis the AC system of the experimental hall [7]. The results verified the insufficient cooling capacity and proposed AC improvement plan. We had accomplished the AC improvement project at the end of 2005. Measurements and numerical simulation of the improved AC system in the experimental hall were conducted.

Air Conditioning System Improvement

The abovementioned AC system improvement of the experimental hall was implemented by increased the cooling capacity. Two new AHUs were installed to replace the old ones. Specifications of the old and new AHUs are list in the Table 1. The cooling capacity was increased more than tow times.

Table 1: Specifications of the old and new AHUs for the experimental hall

	Air flow (cfm)	Fan(RPM)	Fan static pressure (in WG)	Motor(HP)	Cooling water heat exchange area (ft^2)
Old AHU	12800	1962	3.5	20	26.9
New AHU	30000	914	3.5	30	40.4

2. Measurement Apparatus and Data Acquisition System

Utility Archive System

We had developed a utility archive system to on line monitor many kinds of utility parameters. Although each of the utility subsystem, such as the electrical power system, cooling water system, AC system etc. is equipped with its own system and optimal control logic and completed control system, the utility archive system still successfully integrates all the subsystems.

The utility archive system is a integrated software written by the LabView language. There are four levels of machine server, archive server, mirror server and archive viewer integrated in the archive system. Machine server serves for the data acquisition, format unification and data saving. Each subsystem has its own archive server and the mirror is opened for outside users. Archive viewer is software of data acquisition for the whole archive system. Figure 1 is structure of the utility archive system.

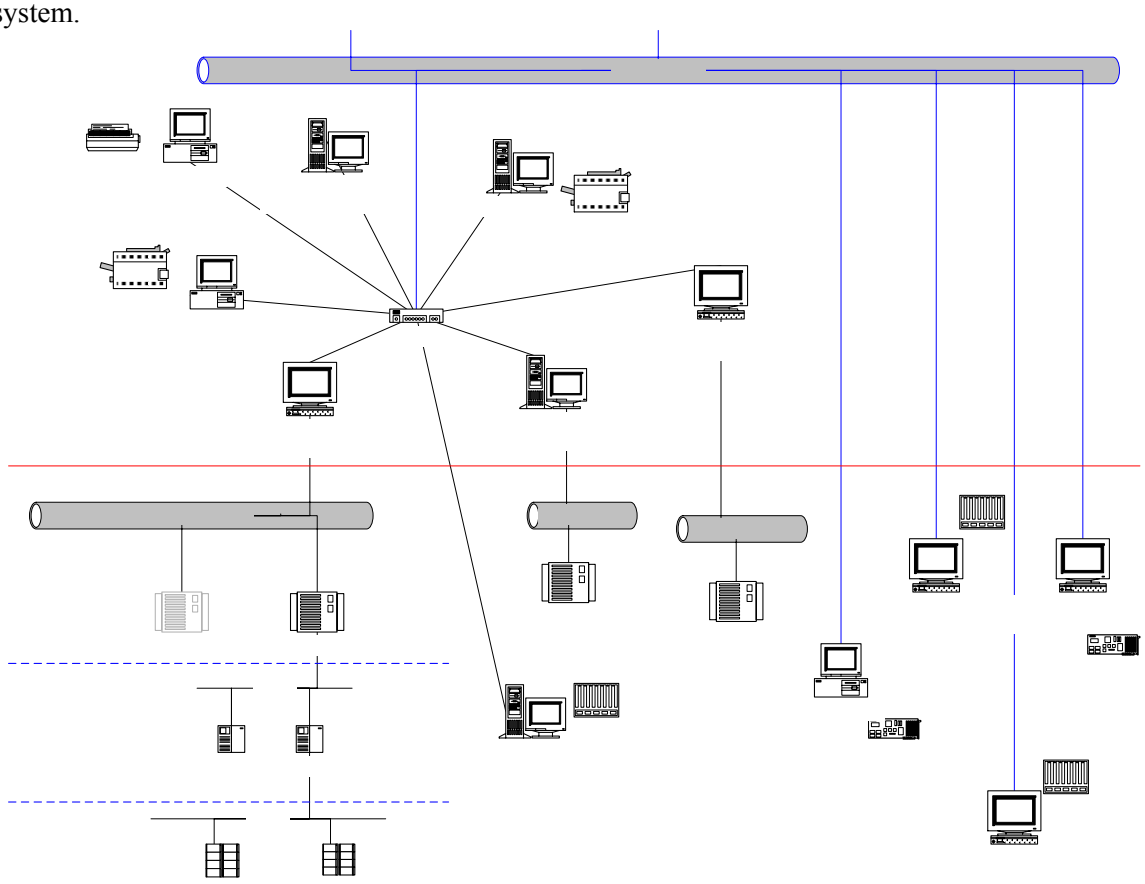

Figure 1: Structure of the utility archive system.

Temperature and Flow Rate Measurement

To on-line control and monitor the air temperature of the experimental hall, we install two to five temperature sensors of PT100 on some specific beamline, as shown in Figure 2. Those temperature sensors are numbered on Figure 2. Also, twelve temperature sensors are installed on the outer wall of the experimental hall. The temperature histories of these seventy-two locations are on-line recorded on the archive system.

The air flow rate was measured by the TSI flow meter of 8373-M-GB AccuBalanve Plus type. The measurement range is 50~3500m^3/h with ±5% precision. The flow velocity at the air exit was measured by the hot wire equipped in the Testo 400 multi-meter. The measurement range is 0~10 m/s, -20~70 ^oC.

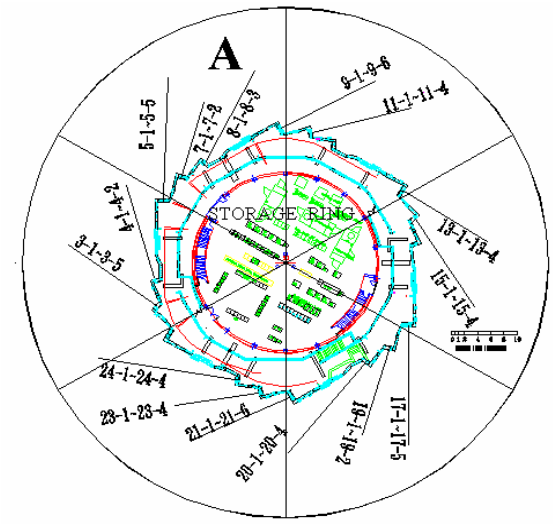

Figure 2: Storage ring layout and temperature sensors distribution.

3. Numerical Simulation

Both cases of the temperature distribution and flow fields before and after the AC system improvement are numerically simulated in this study. We use FLUENT 6.2, a CFD code, to perform the numerical simulation. FLUENT is composed of three parts, pre-processor, core operation and post-processor. GAMBIT, an integrated pre-processor, is used for geometry modelling and grid generation. The basic governing equations include the continuity equation, the momentum equation and the energy equation. The FLUENT solver can model many kinds of fluid dynamics and heat transfer problems. We set our simulated model as a 3D, incompressible and turbulent flow in this study. Both steady-state and transient flows are simulated. We apply the *k*-ε turbulence model and SIMPLEC to solve the velocity and pressure problem.

Model Construction and Grid Generation

Because the whole space of the experimental hall is too large to simulate and the simulation may consumes too much memory, the geometry modelling is simplified. We divide the experimental hall as periodically symmetric six sections, as shown in Figure 2 and assume periodic boundary condition for each section. Then we simplify the simulation by only simulating section A as shown in Figure 2 and apply the results to other five sections.

There are two beamlins located in this area. Also, the geometry of the beamline, rack and other experimental apparatus are simplified to reduce the amount of time. The circular air exits with 0.32m in diameter are distributed on the ceiling. The air exhausts of 1m × 0.5m in dimension are located on middle of the inner wall. As shown in Figure 3, brown spots on the ceiling and blue rectangles on the inner wall are air exits and exhausts, respectively.

Grid size is another critical parameter in the simulation. Too big grid size may lose the precision of the simulation while too small grid size may result in too much computing memory and time. Total 629,524 tetrahedron grids with 0.32m-edge are generated in the simulated area as shown in Figure 3.

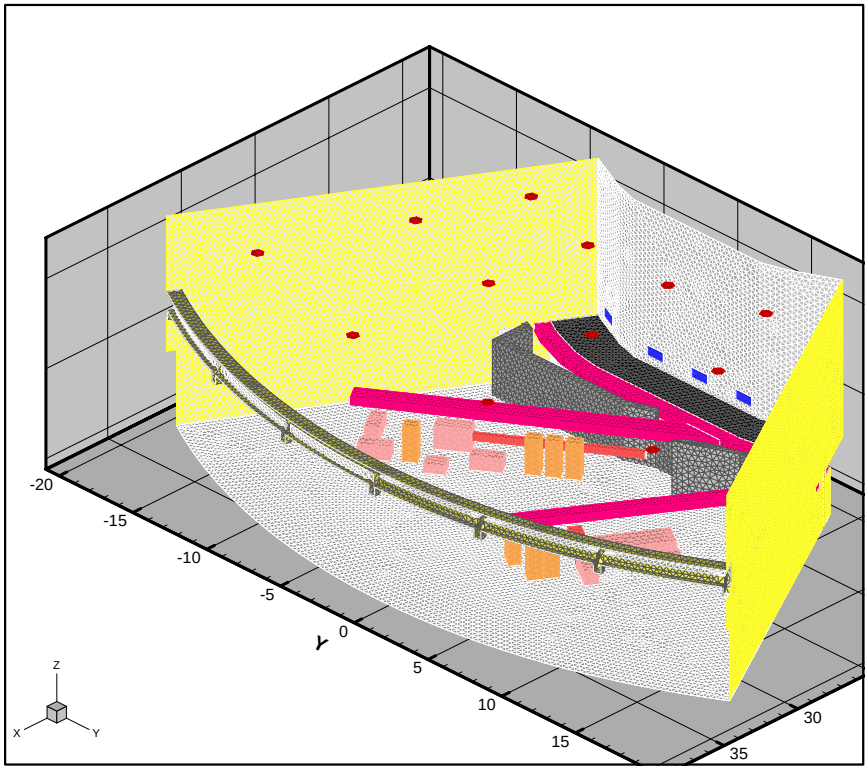

Figure 3: Physical model and grid structure of the simulation.

Boundary Condition

The boundary condition of the simulation is based on results of the actual measurements. The air velocities before and after the abovementioned AC improvement are measured by using the hot wire equipped in the Testo 400 multi-meter. The heat flux from the ceiling is calculated according to the ASHRAE Handbook Fundamentals [8]. All the boundary conditions are list in the Table 2.

Table 2:Boundary conditions for the CFD simulation.

Air exit (On the ceiling)	Air velocity (before improvement)	1.34 m/s
	Air velocity (after improvement)	5.39 m/s
	Temperature	14.2 ^{o}C
Heat flux from the ceiling		30.7 W/m^2
Heat source	Beamline and human	1.68 W/m^3
Computer		37 ^{o}C
Rack		35 ^{o}C
Wall and floor		Adiabatic

Convergence Criterion

Because of the truncation error of the numerical computation and the differences of computed values resulted from the iteration, there exists small difference between two sides of the governing equation. This difference is known as the residual value. The residual value is used as the index of the

convergence criterion in the numerical simulation. All the residual values of all physical parameters are set as $1\times 10^{-6.}$ If the residual value is not larger than 1×10^{-6}, the iteration is considered convergent.

4. Results and Discussion

Measurements Results

Figure 4 shows four days' outdoor atmosphere and indoor air temperature histories (A) before and (B) after the AC improvement. Six temperature histories respectively at BL 5-1, BL 5-2, BL 7-1, BL 7-2, BL 8-1 and BL 8-2, as shown in Figure 2, are recorded in Figure 4. Figures 4(A) and 4(B) were recorded at end of April of 2005 and 2006, respectively. Both outdoor air temperature histories ranged about from 20 °C to 30 °C in Figure 4. Before the AC improvement, both temporal and spatial variations of indoor temperature histories are about 1.2 °C and the temperature fluctuations during ten minutes ranged from 0.2 °C to 0.5 °C depending on the location, as shown in Figure 4(A). All the temperature variations and fluctuations were improved after the AC system improvement. As shown in Figure 4(B), both temporal and spatial variations of indoor temperature histories are about 0.6 °C and the temperature fluctuations during ten minutes ranged from 0.1 °C to 0.2 °C.

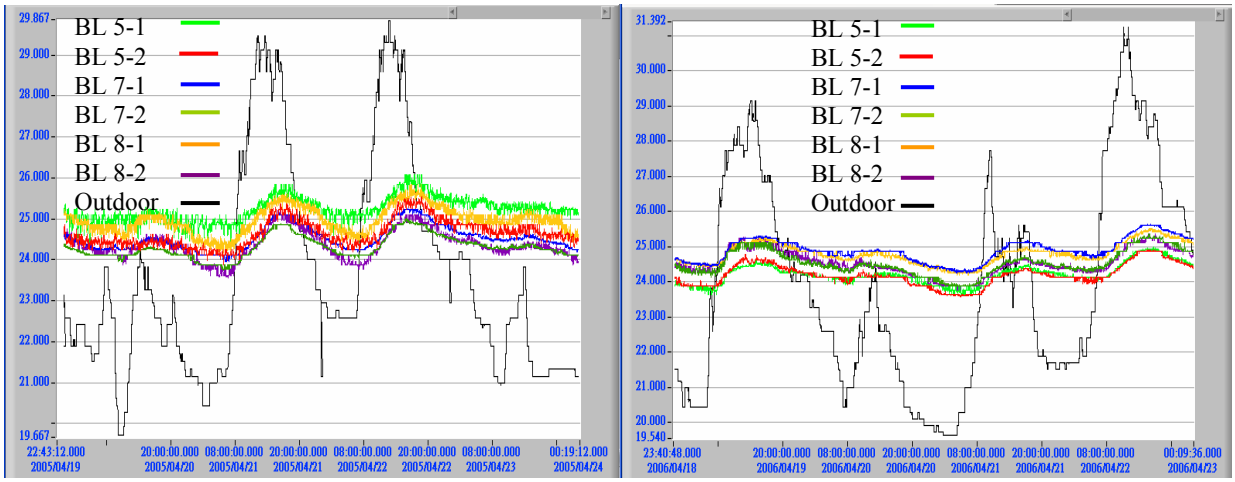

(A) (B)

Figure 4: Outdoor atmosphere and indoor air temperature histories (A) before and (B) after the AC improvement.

Table 3 shows the flow rate and air velocity before and after the AC system improvement. Basically, the flow rate and air velocity are spatially uniform. The average flow rates before and after the AC system improvement are 105 L/s and 432 L/s, respectively. Thus the flow rate was increased about 3 times after the AC improvement. The average air velocities before and after the AC system improvement are 1.34 m/s and 5.39 m/s, respectively. These two numbers are also list in Table 2 as the boundary conditions for the CFD simulation.

Table 3:Flow rate and air velocity before and after the AC system improvement.

No.		1	2	3	4	5	6	7	8	9	Ave
Before AC improvement	Flow rate (L/s)	102	98	117	106	100	109	119	92	101	105
	Air velocity (m/s)	1.38	1.28	1.44	1.32	1.23	1.34	1.53	1.25	1.29	1.34
After AC improvement	Flow rate (L/s)	423	408	483	438	412	430	492	393	405	432
	Air velocity (m/s)	5.42	5.22	5.57	5.30	5.08	5.44	6.38	4.92	5.16	5.39

Numerical Simulation Results

Figures 5 and 6 show the simulated temperature field of the experimental hall before and after the AC system improvement, respectively. Basically, the temperature of the whole experimental may be divided into upper and lower zones. The average temperature of the upper zone is lower because the cooling air exits are distributed on the ceiling. On the contrary, the temperature of the lower zone, is

higher due to the heat source of beamlines and experimental apparatus, as shown in both Figures 5 and 6.

Although the temperature of the upper zone is lower, there is thin layer of high temperature near the ceiling resulted from the ceiling heat flux, as shown in both Figures 5 and 6. Because the cooling air flow rate from the air exits is increased about three times after the AC system improved, the average air temperature shown in the Figure 6 is obviously lower than that shown in the Figure 5.

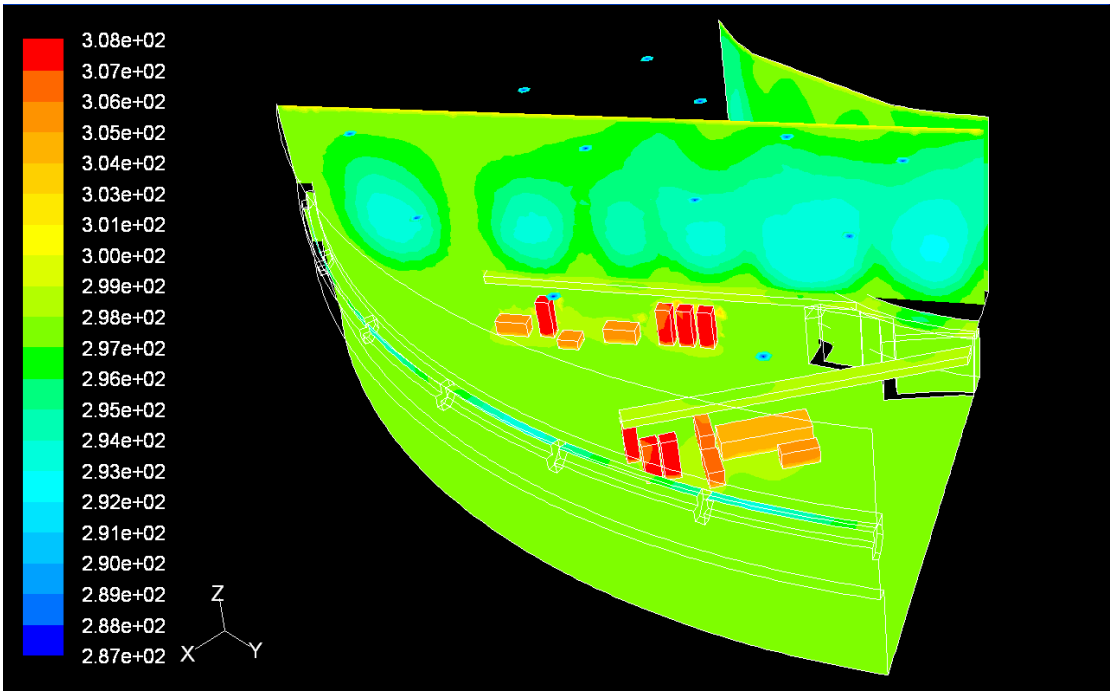

Figure 5 Simulated temperature field of the experimental hall before the AC system improvement.

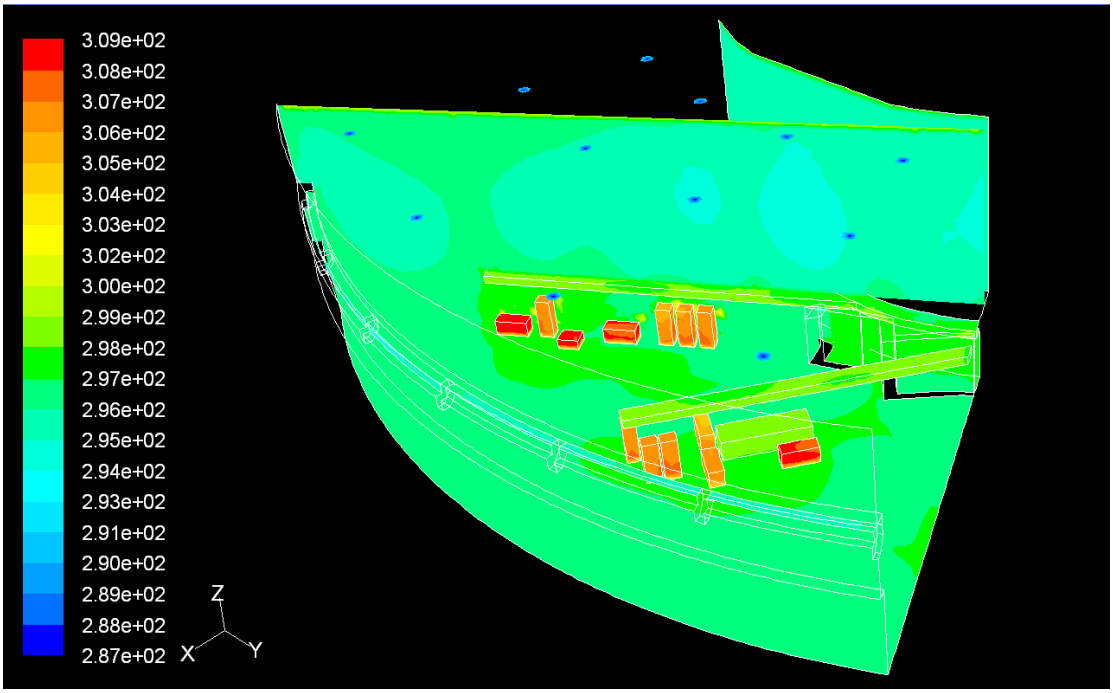

Figure 6 Simulated temperature field of the experimental hall after the AC system improvement.

Figure 7 demonstrates the simulated cross-sectional flow field of the experimental hall after the AC system improvement. The air flow velocities range from 0-2 m/s, as shown in the figure. Velocity of one area with arrow in blue color is higher than velocity of other area because the area is near an air exit. Several flow circulations appear clearly in the figure. Those circulations are also show low temperature in the Figure 6.

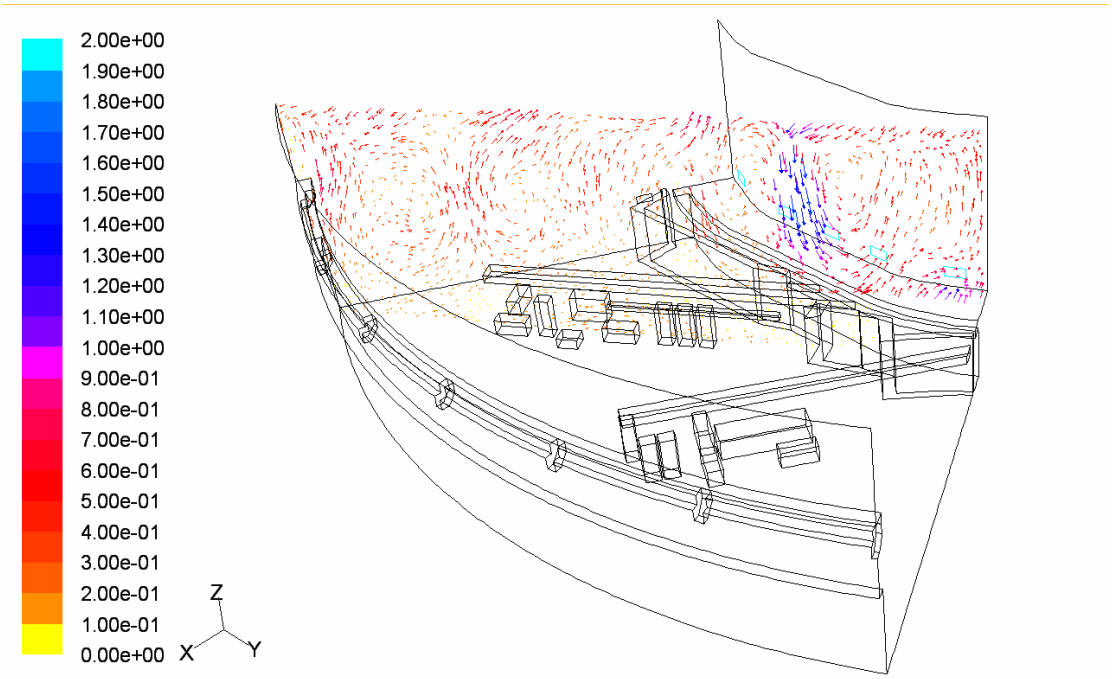

Figure 7 Simulated cross-sectional flow field of the experimental hall after the AC system improvement.

In order to simulate the transient state of the temperature field of the experimental hall, we modify the boundary conditions of some heat sources. as list in Table 4. We also select some points along the two beamlines near locations of temperature sensors installed as shown in Figure 2 to examine simulated temperature temporal variations. The simulated results show that the temperature temporal variation before and after the AC system improvement range from ±0.15 ^{o}C to ±0.10 ^{o}C and from ±0.10 ^{o}C to ±0.07 ^{o}C, respectively. The simulated results of the temperature variations are smaller than the actual measured data and list in Table 5.

Table 4:Boundary conditions for the CFD transient simulation.

Heat source	Beamline and human	1.68+0.2cos(0.1t) W/m^3
Computer		37+0.2cos(0.1t) ^{o}C
Rack		35+0.2cos(0.1t) ^{o}C

Table 5: Simulated temperature variation before and after the AC system improvement.

Point location	Simulated temperature variation before the AC improvement	Simulated temperature variation after the AC improvement
Beamline 5-1	±0.15 ^{o}C	±0.10 ^{o}C
Beamline 5-2	±0.13 ^{o}C	±0.08 ^{o}C
Beamline 5-3	±0.12 ^{o}C	±0.08 ^{o}C
Beamline 5-4	±0.10 ^{o}C	±0.07 ^{o}C
Beamline 8-1	±0.15 ^{o}C	±0.10 ^{o}C
Beamline 8-2	±0.11 ^{o}C	±0.07 ^{o}C

5. Conclusion Remarks

The AC system improvement for the experimental hall had been accomplished to increase the cooling capacity about three times at the end of 2005. The experimental measurements are conducted to collect the temperature histories through the Archive system and data of air flow rates and flow velocities at air exits. The collected data show that the average temperature temporal variation is reduced from 1.2 ^{o}C to 0.6 ^{o}C. The average air flow rate and flow velocity are increased about three times.

The numerical simulation of the temperature distribution and the flow field of both steady and transient states before and after the AC system improvement are performed. The simulated results of steady state show that the temperature of the whole experimental hall may be divided into upper and lower zones. The average temperature of the upper zone is lower due to the supplied cooling air while the temperature of the lower zone is higher due to the heat source of experimental apparatus. The simulated results of transient state demonstrate the same trend of the temperature variation with the actual measured one but the simulated values are smaller than the actual collected data.

6. Acknowledgement

The authors would like to thank the colleagues of the utility group of NSRRC for their assistance.

References

[1] J.R. Chen, H.M. Cheng, Z.D. Tsai, C.R. Chen, T.F. Lin, G.Y. Hsiung, and Y.S. Hong, "The Correlation between the Beam Orbit stability and the Utilities at SRRC", Proc. of 6th European Particle and Accelerator Conference EPAC98, Stockholm, Sweden, June 22-26, 1998.

[2] J.R. Chen, D.J. Wang, Z.D. Tsai, C.K. Kian, S.C. Ho, and J.C. Chang, "Mechanical Stability Studies at the Taiwan Light Source", 2nd Int'l Workshop on Mechanical Engineering Design of Synchrotron Radiation Equipment and Instrumentation (MEDSI02), APS, U.S.A., Sep 5-6, 2002.

[3] D.S. Lee, Z.D. Tsai, J.R. Chen and C. R. Chen, "Cooling Air Flow Induced Thermal Deformation of the Magnet Lattice Girder", Proceedings of European Particle Accelerator Conference EPAC2000, Vienna, Austria, June 26-30, 2000.

[4] D.S. Lee, Z.D. Tsai, and J.R. Chen, "Mini Environment Control for the Elliptical Polarization Undulator" 2001 Particle and Accelerator Conference (PAC), June 18-22, 2001, Chicago, USA.

[5] J.C. Chang, C.Y. Liu, and J.R. Chen, "Air Temperature Control Improvement for the Storage Ring Tunnel" 2003 Particle and Accelerator Conference (PAC), May 12-16, 2003, Portland, USA.

[6] J.C. Chang, J.R. Chen, Z.D. Tsai and M. T. Ke "Air Temperature Analysis and Control Improvement for the Storage Ring Tunnel" 2005 Particle and Accelerator Conference (PAC), May 16-20, 2005, Knoxville, USA.

[7] J.C. Chang, M. T. Ke, C.Y. Liu, and J.R. Chen, "Air Temperature Analysis and Control Improvement for the Large-Scale Experimental Hall" 2004 Asian Particle and Accelerator Conference (APAC), March 22-26, 2004, Gyeongiu, Korea.

[8] ASHRAE Handbook, *Fundamentals*, Chapter 28, 2001.